DOI: 10.31265/6q8as012

ENERGY DISSIPATION IN COMPLEX TIME-DEPENDENT INTERACTIONS

Simon Oman[1], Sanel Avdić[1], Igor Emri[2], Jernej Klemenc[1] and Marko Nagode[1]

[1]University of Ljubljana, Faculty of Mechanical Engineering, 1000 Ljubljana, Slovenia
[2] Zhejiang Tiantie Science&Technology Co., Ltd, Tiantai, Zhejiang, China

ABSTRACT

Granular damping elements (GDEs) are promising tunable systems for energy absorption, vibration isolation, and damping applications. Their behaviour is governed by complex particle–particle interactions, including frictional sliding, inelastic collisions, and the formation of force-chain networks. This study investigates the influence of particle properties and casing stiffness on the static and dynamic response of GDEs using a combined approach of Discrete Element Method (DEM) simulations and experiments. Numerical simulations were conducted on monodisperse assemblies of metallic-like and polymer-like particles with varying diameters. The results show that energy dissipation is strongly linked to the evolving contact network topology, coordination number, sliding ratio, and particle compliance. Although softer particles exhibit higher absolute energy dissipation due to increased deformation, the specific damping capacity remains relatively consistent across cases, suggesting that frictional contact mechanics dominate the dissipation process. Experimental tests were performed using catenoidal thermoplastic polyurethane (TPU) casings of different wall thicknesses filled with glass beads. The results indicate that casing stiffness significantly influences both dynamic stiffness and damping behaviour. More compliant casings allow greater relative particle motion, leading to increased energy dissipation. However, they also exhibit higher dynamic stiffness, which in turn affects the system's natural frequency. Overall, the findings demonstrate that dynamic stiffness and damping in GDE systems are inherently coupled and cannot be independently optimised. These results provide valuable insights for the design of next-generation granular damping systems with enhanced and tunable energy dissipation performance.

INTRODUCTION

Energy absorption and dissipation are leading mechanisms behind many beneficial technologies. Their use in critical systems (transportation, industrial machinery, power plants, etc.) and infrastructure (buildings, roads, railways, etc.) is foundational to enhancing safety, performance, efficiency, and well-being in modern society. Nonetheless, existing state-of-the-art technologies often fall short in at least one of the key areas: performance, efficiency, sustainability, and adaptability. These systems frequently have limited energy absorption and dissipation capabilities, are typically made from non-recyclable materials, and have a narrow scope of applicability. The economic impact of these inefficiencies is significant, with losses from earthquakes, vibration-related industrial downtime, reduced turbine efficiency, transport disruptions, and health-related costs collectively reaching billions to hundreds of billions of dollars.

Tunable granular damping elements (GDEs) represent a transformative approach to energy absorption and dissipation. As an emerging class of new damping systems generation, they can be specifically tailored to achieve desired behaviour: shock absorption, energy dissipation, sound insulation, vibration isolation and damping, energy harvesting and so on. GDEs are structured assemblies of particles that interact through contact forces, which can include elastic, plastic, frictional, or dissipative interactions[1,2] and can also provide load-bearing capacity via tunable mechanical properties such as elastic, shear, and bulk moduli[3]. By adjusting particle size, shape, material, and arrangement, their behaviour can be effectively "programmed" under external loading. In some configurations, granular materials enclosed in elastic containers have demonstrated up to 10× improvements in vibration damping compared to current state-of-the-art solutions[3].

GDEs have broad potential across civil engineering (earthquake protection and infrastructure damping), transportation (rail vibration reduction), manufacturing (machine isolation), automotive and aerospace (crash protection and adaptive damping), defence (blast mitigation), medical devices (prosthetics and surgical tools), and energy systems (improved turbine stability and energy harvesting). They also support green transition[4] and circular economy goals by enabling reuse of waste materials such as tires, conveyor belts, and composites, as well as the use of abundant natural granular materials like gravel.

Compared to metamaterials with complex geometries or polymer-based damping systems, GDEs rely on force chain formation, friction, inelastic particle collisions, and internal material dissipation like shown in Fig. 1. **Energy dissipation in GDE systems emerges from transient evolution of force-chain topology under constrained relative particle motion**. Therefore, by simply filling elastic structures with granules can significantly enhance energy absorption and dissipation. Prior research on granular damping systems has shown 10–100× performance improvements[5] over bulk material approaches due to pressure-dependent changes in stiffness and damping within confined granular media. However, accurately predicting and optimizing custom-designed GDE behaviour still requires deeper understanding of their underlying mechanisms.

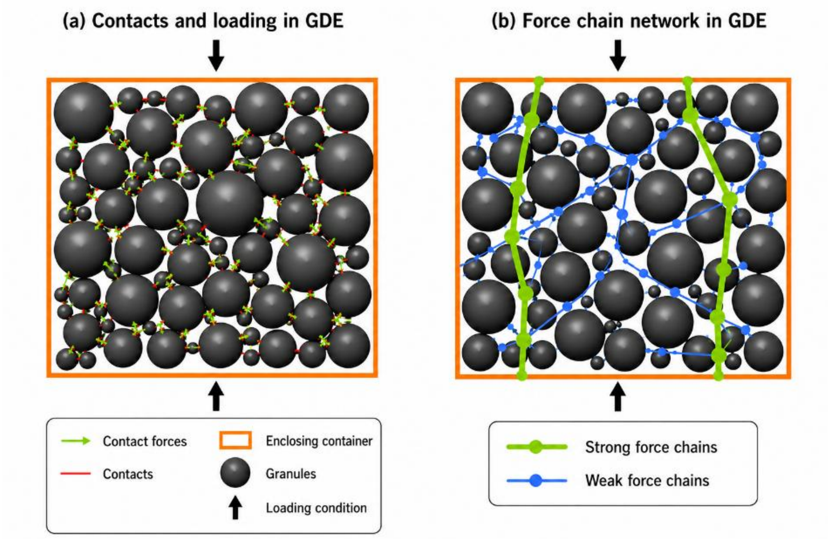

FIGURE 1: Main energy absorbing and damping mechanisms in GDEs.

This research will present the influence of particle parameters and GDE casing stiffness to the GDE static and dynamic stiffness and damping capabilities. The research is based on DEM simulations in combination with the experimental results.

DEM SIMULATIONS

The numerical analysis consisted of uniaxial compression simulations performed on monodisperse sphere assemblies confined within a rigid cylindrical specimen of 20 mm diameter and approximately 50 mm height, corresponding to an aspect ratio of 2.5. Two materials were considered: metallic-like (M1, E=80 GPa) and polymer-like (M2, E=3.5 GPa), representing a stiff-to-compliant material pair with an elastic modulus ratio of approximately 23. Poisson's ratios were 0.3 and 0.38 for M1 and M2 respectively, and the inter-particle friction coefficient was set to 0.3 for both materials. To enable direct comparison of material effects at equivalent contact network topology, the number of particles was kept the same between both materials for each diameter: 18000 spheres for the 1 mm cases and 2250 spheres for the 2 mm cases. For the polymer-like assemblies (M2), this corresponds to a total mass of approximately 13.4 g for both diameters. For metallic-like assemblies (M1), the identical particle counts yield a substantially higher mass of approximately 74.0 g, reflecting the density ratio of the two materials (7850 kg/m³ versus 1420 kg/m³). For each material and diameter combination, four quantities were extracted from the stabilised fifth loading cycle: assembly stiffness C, specific damping capacity η, coordination number Z, and sliding ratio S. The stiffness is defined as the slope of the loading curve and is calculated based on the maximum and minimum compressive forces (Fmax and Fmin) and displacements (dmax and dmin) of the rigid plate. Specific damping capacity is defined as the ratio of the dissipated energy ΔU (which corresponds to the area enclosed by the hysteresis loop on a force–displacement diagram) and the maximum possible reversible energy of the system U. The coordination number is defined as the average number of contacts per particle, while the sliding ratio represents the fraction of sliding contacts (contacts for which the tangential force exceeds the Coulumb sliding treshlod). Together, these four parameters provide a coupled macroscopic and contact-level characterisation of the dynamic response.

The mechanical response of the four granular assemblies was characterised through force-displacement (F-d) curves recorded over five uniaxial compression cycles. Assembly stiffness and specific damping capacity were extracted from the stabilised fifth cycle, while the coordination number and sliding ratio were tracked as functions of applied compression force to provide contact-level insight into the observed macroscopic behaviour.

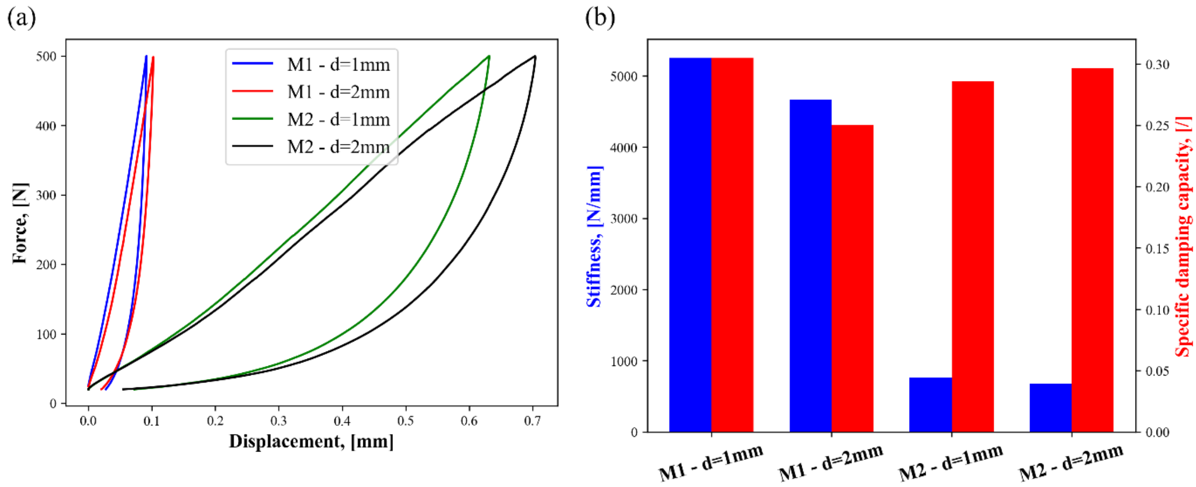

FIGURE 2: (a) Force-displacement curves, (b) stiffness and specific damping capacity

The F-d curves in Figure 2(a) reveal a strong material dependence in both compliance and energy dissipation. M1 assemblies exhibit near-vertical loading branches, reaching 500 N within approximately 0.092 mm (1 mm) and 0.11 mm (2 mm), while M2 assemblies require displacements up to 0.63 mm and 0.70 mm, respectively. The substantially wider hysteresis loops of M2 immediately suggest higher energy dissipation per cycle, yet the quantified specific damping capacity given in Figure 2(b) reveals that η values range only from 0.250 to 0.305 across all four cases. This narrow spread indicates that the dissipation fraction, energy lost relative to maximum potential elastic energy, is governed primarily by contact-level friction mechanics rather than bulk compliance, since the large difference in stiffness between M1 and M2 does not translate into a proportionally large difference in specific damping capacity. The absolute energy dissipated per cycle is, however, far greater for M2 due to its much larger displacement amplitude at the same force level.

The stiffness shows a clear material-driven hierarchy (M1 approximately seven times stiffer than M2) and a consistent, material-independent size effect, 1 mm assemblies are approximately 12% stiffer than their 2 mm counterparts for both materials. This size effect is directly correlated with the coordination number data in Figure 3(a), where 1 mm assemblies maintain higher *Z* values throughout loading, reaching approximately 4.55 versus 4.30 for M1, and 5.25 versus 5.00 for M2 at 500 N. The denser contact network in smaller-particle assemblies provides more parallel load-bearing paths, explaining the stiffness increase. Importantly, M2 assemblies exhibit consistently higher coordination numbers than M1 across the entire loading range. This reflects the greater compliance of M2 contacts. At any given force level, M2 contacts deform more, increasing the likelihood of new contact formation and sustaining a richer force-chain network.

The coordination number data also explain the evolution of the sliding ratio in Figure 3(b). All assemblies show a sharp drop in sliding ratio from approximately 0.26–0.28 at 5 N to a minimum near 0.14–0.16 at 100 N. This transition coincides with the steep rise in *Z* in the same force range, confirming that rapid contact formation redistributes the applied load across an expanding network, bringing individual contacts away from their Coulomb sliding threshold. Beyond 100 N, *Z* grows more gradually and the sliding ratio recovers steadily, indicating that newly formed contacts are progressively loaded toward sliding. Critically, M1 assemblies reach significantly higher sliding ratios at peak compression (~0.23–0.24) compared to M2 (~0.14–0.18).

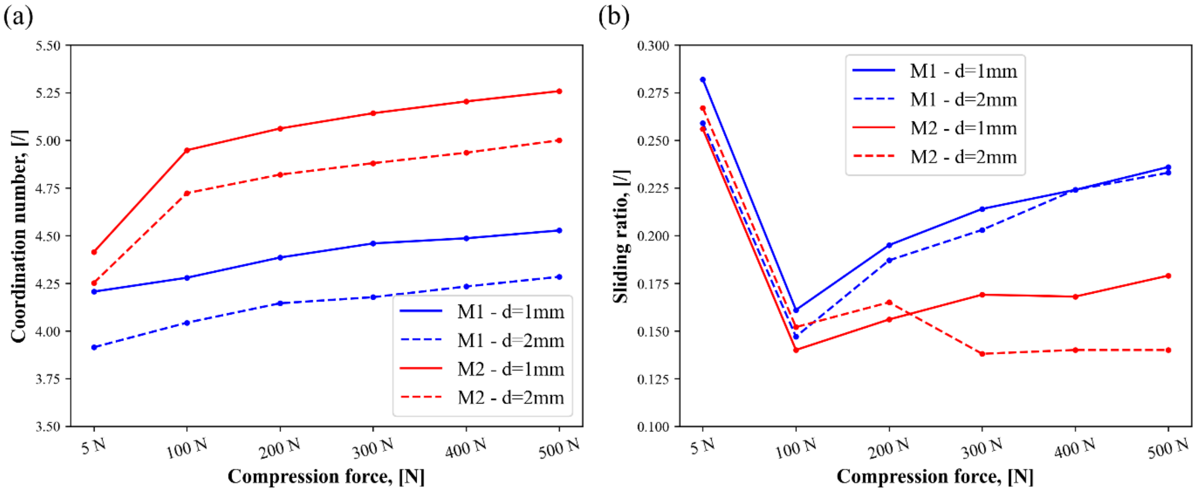

FIGURE 3: (a) Coordination number, (b) sliding ratio

This inverse correlation between coordination number and sliding ratio across the two materials is physically consistent, suggesting that the higher *Z* in M2 distributes load more uniformly, keeping a greater fraction of contacts below the frictional limit. For M1, the lower *Z* concentrates force on fewer contacts, driving more of them into sliding which is a mechanism that directly links contact network topology to frictional activity. The relationship between contact network topology and η is clearest within the M1 assemblies. Despite M1 d=1 mm and M1 d=2 mm exhibiting nearly identical sliding ratios at peak load (~0.23), their specific damping capacities differ noticeably (0.305 versus 0.250). This is better explained by their coordination numbers: the higher *Z* of the 1 mm assembly (~4.55 versus ~4.30 at 500 N) provides more active contacts contributing to micro-slip, increasing the total dissipated energy without a proportional increase in stored energy. For M2 assemblies, the size effect operates differently: M2 d=2 mm has both a lower sliding ratio and lower Z than M2 d=1 mm at peak load, yet records the higher η (0.297 versus 0.286). Here the greater contact deformation of the more compliant 2 mm spheres amplifies the tangential micro-slip amplitude at each contact, offsetting the sparser contact network. Taken together, these results indicate that specific damping capacity is not controlled by a single contact-level quantity, but by the interplay between contact network density, captured by coordination number, and per-contact deformation, which scales with particle compliance.

EXPERIMENTAL SECTION

The numerical DEM results show that the amount of dissipated energy within the GDE element is strongly related to its stiffness. In our previous studies[6] we demonstrated that the magnitude of dissipated energy is most significantly influenced by friction between the granules as well, which simultaneously also affects stiffness. For this reason, optimal specific damping capacity requires an appropriate level of friction that enables good flowability, or relative movement between the granules during loading, while at the same time ensuring sufficient energy loss due to sliding between them.

To increase the possibility of relative movement between the granules during loading, it is necessary to provide an elastic casing for the GDE element. Since the DEM analysis presented in the previous chapter does not allow simulations with elastic boundary elements, this chapter presents the influence of casing stiffness on the dynamic stiffness and the specific damping capacity of the GDE through experimental results.

To show the influence of the stiffness of the GDE casing on its characteristics a catenoidal shape of GDE casing with three different thicknesses (0.8, 1.2 and 1.6 mm) was selected and experimentally validated. GDE casings were 3D printed from soft TPU material and filled with glass beads of Mesh #20 size with some additional Vaseline added to decrease the friction between the beads. Simple 3D printed parts were used to cover the bottom part of the GDE casings after filling it with granulate. Bottoms were glued to TPU casings using a super glue. The shape of the sample is presented in Figure 4.

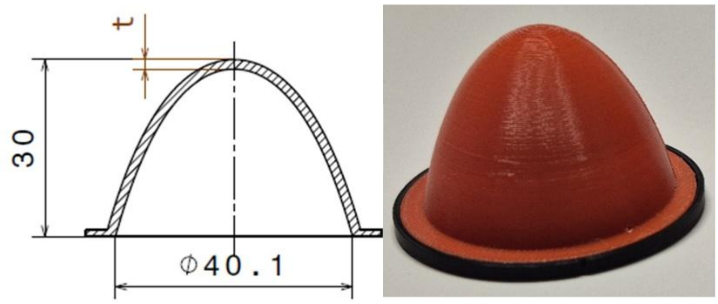

FIGURE 4: Shape of GDE element used for experimental evaluation

To check how dynamic stiffness and specific damping capacity change with static preload, several different preloads have been used (50, 100, 150, 200, 250, 300, 400, 500 and 600 N) on which cyclic loading with constant displacement amplitude of 0.125 mm has been added (10 cycles at each preload). The processed experimental results are shown in two graphs in Figure 5.

Results for all investigated specimens show that dynamic stiffness increases progressively with the preload. Due to the progressive characteristics of the catenoid, such results are expected. If we look more closely at the specific damping capacity results, we can find that it is maximal at a specific preload of the test specimen, which, however, varies from test specimen to test specimen. A closer examination of the obtained results reveals that the optimal specific damping capacity for a given catenoidal shape occurs at approximately the same static height. However, since the static stiffness is conditioned by the thickness of the shell, the optimal height for samples with different thicknesses is obtained at different static loads. The optimal preload height for used shape is around 21 mm (9 mm compressed sample).

If specific damping capacities are further compared, it is observed that the highest values are found in the samples with the lowest wall thickness, which are also characterized by the greatest elasticity in terms of their static behaviour. Combining these findings, we can conclude that in order to ensure the optimal shape and consequently characteristics (best specific damping capacity), it is important to properly adapt the damping element to the static load, which can be done by optimizing the thickness and geometry of the GDE casing or the stiffness of the material from which it is made.

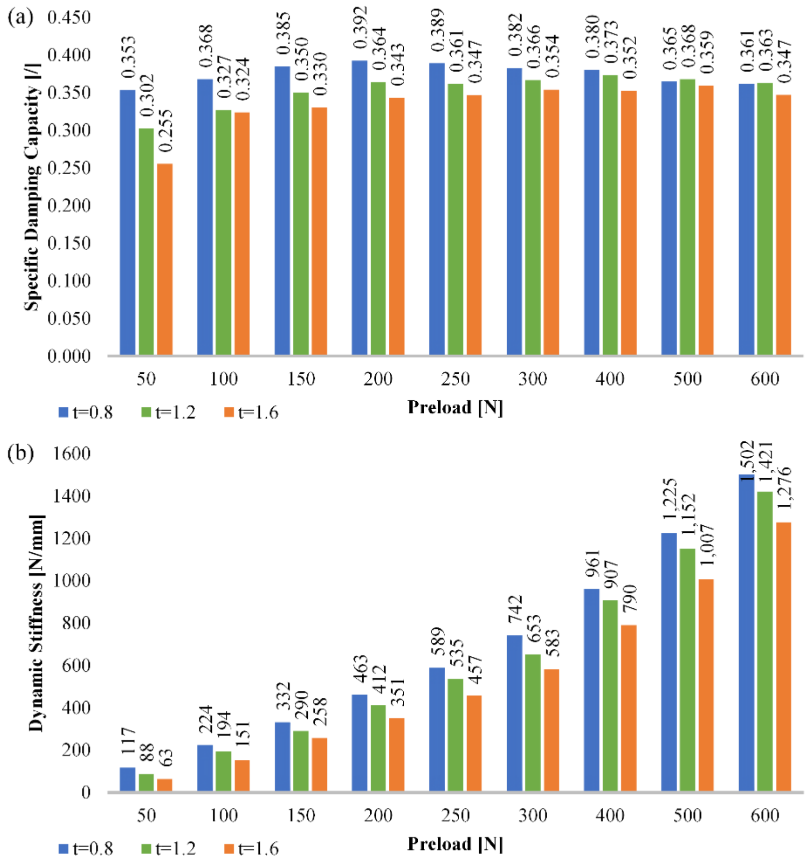

FIGURE 5: Experimental results: (a) Specific Damping Capacity, (b) Dynamic Stiffness

A very important finding from these results is that the dynamic stiffness of samples with lower static stiffness is higher than those with higher static stiffness. This is partly related to the fact that the height of the sample on which the dynamic loading is performed is different between samples. For samples with lower static stiffness, it is already shifted more into the progressively increasing part of the stiffness curve, while for samples with higher static stiffness it can remain in the flatter part of the curve. The second part for this phenomenon is related to the fact that in samples with lower stiffness the proportion of damping compared to stiffness is higher, which results in much steeper unloading curve of the Force-Displacement characteristic and consequently higher dynamic stiffness. This indicates that stiffness and damping are closely related and therefore cannot be independently controlled at the level of an individual GDE element.

CONCLUSIONS

This study investigated the energy dissipation mechanisms and dynamic behaviour of granular damping elements (GDEs) using a combination of DEM simulations and experimental analysis. The obtained results demonstrate that the damping performance of GDE systems is governed by the complex interplay between particle-scale contact mechanics and the global stiffness of the enclosing structure. The presented results also indicate that the behaviour of granular damping systems cannot be fully understood through bulk constitutive descriptions alone, but requires explicit consideration of evolving contact-network topology and constrained particle kinematics.

The numerical simulations showed that the amount of dissipated energy is strongly related to the contact network topology, coordination number, sliding ratio, and particle compliance. Softer materials exhibit significantly larger deformation amplitudes and therefore greater absolute energy dissipation. However, the specific damping capacity is governed predominantly by frictional interactions at particle contacts, indicating that the damping behaviour originates primarily from transient internal reconfiguration processes within the granular contact network.

The experimental investigation confirmed that the stiffness of the elastic GDE casing has a major influence on the dynamic response of GDE elements. Softer casings allow greater relative movement between granules, resulting in improved specific damping capacity. The results further revealed that the optimal specific damping capacity is achieved at a specific static preload level corresponding to an optimal compressed height of the element. This indicates that the geometry, wall thickness, and material properties of the casing must be carefully adapted to the expected operating conditions.

An important finding of this work is that specific damping capacity and dynamic stiffness are strongly coupled properties and therefore cannot be independently controlled at the level of an individual GDE element. Consequently, achieving optimal performance requires simultaneous optimization of particle properties, inter-particle friction, particle size, casing geometry, and casing stiffness.

The presented results contribute to a better understanding of complex time-dependent interactions in granular systems and provide a foundation for the development of advanced tunable damping solutions for applications in civil engineering, transportation, manufacturing, energy systems, and vibration-sensitive technologies.

ACKNOWLEDGMENTS

The authors would like to thank the Slovenian Research Agency (P2-0182, Development evaluation) and Zhejiang Tiantie Industry Co Ltd for providing financial and material support.

REFERENCES

1. Jaeger, H.M.; Nagel, S.R. Physics of the Granular State. Science 1992, 255, 1523–1531.
2. Venkatesh, R.; Brojan, M.; Emri, I.; Voloshin, A.; Govekar, E. Influence of Particle Size Distribution Width on GFA Index of Uniaxially Compressed Granular Materials. Powder Technology 2021, 377, 666–675.
3. Gosar, A.; Emri, I.; Klemenc, J.; Nagode, M.; Oman, S. On the Vibration-Damping Properties of the Prestressed Polyurethane Granular Material. Polymers 2023, 15, 1299.
4. Plastic pollution is growing relentlessly as waste management and recycling fall short, says OECD | OECD
5. Avdić, S.; Nagode, M.; Klemenc, J.; Oman, S. Experimental Evaluation of a Granular Damping Element. Polymers 2024, 16, 1440.
6. Avdić, S.; Nagode, M.; Klemenc, J.; Emri, I.; Oman, S. The influence of inter-particle friction on multiscale response of uniaxially loaded granular material. Journal of Materials Research and Technology 2025, 38, 3208-3217.